Article

Electrophysiological signatures underlying variability in human memory consolidation

Wei Duan[1,2,8], Zhansheng Xu[3,4,8], Dong Chen [1,2], Jing Wang[5], Jiali Liu[1,2], Zheng Tan[1,2], Xue Xiao[1,2], Pengcheng Lv[1,2], Mengyang Wang[5], Ken A. Paller [6], Nikolai Axmacher [7] & Liang Wang [1,2] ✉

We experience countless pieces of new information each day, but remembering them later depends on firmly instilling memory storage in the brain. Numerous studies have implicated non-rapid eye movement (NREM) sleep in consolidating memories via interactions between hippocampus and cortex. However, the temporal dynamics of this hippocampal-cortical communication and the concomitant neural oscillations during memory reactivations remains unclear. To address this issue, the present study used the procedure of targeted memory reactivation (TMR) following learning of object-location associations to selectively reactivate memories during human NREM sleep. Cortical pattern reactivation and hippocampal-cortical coupling were measured with intracranial EEG recordings in patients with epilepsy. We found that TMR produced variable amounts of memory enhancement across a set of object-location associations. Successful TMR increased hippocampal ripples and cortical spindles, apparent during two discrete sweeps of reactivation. The first reactivation sweep was accompanied by increased hippocampal-cortical communication and hippocampal ripple events coupled to local cortical activity (cortical ripples and high-frequency broadband activity). In contrast, hippocampal-cortical coupling decreased during the second sweep, while increased cortical spindle activity indicated continued cortical processing to achieve long-term storage. Taken together, our findings show how dynamic patterns of item-level reactivation and hippocampal-cortical communication support memory enhancement during NREM sleep.

Sleep can facilitate the consolidation of newly encoded information, thus producing long-lasting memories. At the neural level, this process relies on neural oscillations (in particular, thalamo-cortical sleep spindles and hippocampal sharp wave-ripples), reactivation of memory traces, and hippocampal-neocortical interactions[1–4]. Although humans encounter countless pieces of information every day, only a small subset remains available to be remembered later. Emerging evidence suggests that sleep-dependent memory consolidation is not a passive process but actively supports memory storage[5–8]. Importantly, however, not all encoded information is consolidated equally,

[1]State Key Laboratory of Cognitive Science and Mental Health, Institute of Psychology, Chinese Academy of Sciences, Beijing, China. [2]Department of Psychology, University of Chinese Academy of Sciences, Beijing, China. [3]Faculty of Psychology, Tianjin Normal University, Tianjin, China. [4]Key Research Base of Humanities and Social Sciences of the Ministry of Education, Academy of Psychology and Behavior, Tianjin Normal University, Tianjin, China. [5]Department of Neurology, Sanbo Brain Hospital, Capital Medical University, Beijing, China. [6]Department of Psychology and Cognitive Neuroscience Program, Northwestern University, Evanston, USA. [7]Department of Neuropsychology, Institute of Cognitive Neuroscience, Faculty of Psychology, Ruhr University Bochum, Bochum, Germany. [8]These authors contributed equally: Wei Duan, Zhansheng Xu. ✉e-mail: lwang@psych.ac.cn

and some memories are preferentially consolidated[7–10]. Recent studies have started to explore this selective consolidation of specific memories, but the neural mechanisms underlying this process remain poorly understood.

Previous research suggests that this selection process may be triggered by salient tags that are attached to specific memories during encoding to mark important information. One example of such preferred processing is emotional memory. Some studies showed that compared with neutral events, memories of emotional events were reactivated and consolidated with priority[7–9]. Besides that, sleep selectively consolidates memories on the basis of reward information. A human behavioral study found that providing reward expectancy after training improved sleep-dependent memory consolidation[10]. Beyond these pieces of intrinsically valuable information, sensory tags have been used to experimentally manipulate memory consolidation. In the past decade, a powerful method for investigating sleep consolidation—targeted memory reactivation (TMR)—has come to be widely used[11]. In this method, sensory cues (e.g., sound or odor stimuli) are paired with information during learning and then presented again during subsequent sleep. A large number of studies have shown that these sensory cues can reliably influence memory storage[11–14]. In short, endogenous tags based on emotion or reward, or exogenous sensory cues, can systematically improve consolidation during sleep and thus strengthen the corresponding memories. On the other hand, it is worth noting that endogenous and exogenous tags are not necessary for memory reactivation. For example, Schreiner et al. found that memory reactivation can occur without external cues[15].

How does sleep selectively enhance tagged memories? Previous studies suggest that memory reactivation is important for sleep-dependent memory enhancement. Sterpenich et al. showed that compared to non-rewarded events, neural patterns of rewarded events were predominant in N3 stage (slow-wave sleep, SWS), indicating that reward-related tags promote the reactivation of rewarded memories in NREM sleep to enhance their consolidation[7]. Animal and human TMR studies similarly found that sensory cues promote reactivation of cued memories, and the degree of reactivation predicts subsequent memory performance[16–19]. Interestingly, cortical reactivation evoked by a single TMR cue appears to occur in multiple consecutive sweeps and produce a temporal sequence of reactivation[20]. In a rat experiment, a cue-evoked increase of hippocampal replay lasted for 10 s, until another acoustic cue was played[19]. These echoes of reactivation after sensory cues suggest that TMR may strengthen memory traces through reverberation of replay between hippocampus and cortex[12]. In addition, a large number of studies have documented that neural oscillations during NREM sleep, such as thalamocortical spindles and hippocampal ripples, play critical roles in memory consolidation[21–23]. Researchers proposed that ripples continuously retransmit information that has been reorganized or integrated in the hippocampus to the cortex for long-term storage[21,24,25]. This assumption is supported by the evidence that cortical ripples and high-frequency broadband (HFB) activities (i.e., 60–160 Hz) are coupled to the hippocampal ripple events, indicating hippocampal-cortical information communication[24,26,27].

Representational similarity analysis (RSA) has emerged as a powerful tool to identify the formation of stimulus-specific memory traces and their reactivation during subsequent processing stages, including short-term memory maintenance[28] and long-term memory retrieval[29]. In addition, we found recently that stimulus-specific representations reemerged spontaneously in association with ripples during NREM sleep, and that this benefited memory consolidation in humans[3].

The systems consolidation theory hypothesizes that newly encoded memory traces are interactively processed in neocortical and hippocampal networks in order to become stable long-lasting memories[22,30–32]. The existing evidence has demonstrated that TMR procedures can induce hippocampal-cortical functional connectivity change[33–35]. For example, Cousins and colleagues found that TMR significantly enhanced functional connectivity between the caudate nucleus and hippocampus using motor learning task[35] (i.e., serial reaction time task). However, due to the limited temporal resolution of fMRI and the low sensitivity of scalp EEG for activity in deep brain areas, it remains unclear how human hippocampal-cortical interactions changes when cortical reactivation occurs.

It is noteworthy that not all TMR cues have the same effect. For example, TMR effects can be influenced by pre-sleep memory accuracy. TMR benefits for spatial memory were more apparent for weak memories than strong memories[36–40]. This indicates that the categorical comparison of tagged vs. untagged memories may be complicated by other factors that influence whether memories are strengthened. In the present study, we analyzed neural signals that may help explain why some TMR-cued items are preferentially strengthened during sleep.

A key challenge is to precisely characterize brain activity during sleep that is directly related to the enhancement of a specific memory. To face this challenge, we recorded intracranial EEG (iEEG) in patients with medically intractable epilepsy who performed an object-location TMR paradigm. The rare opportunity to directly measure neurophysiological responses in these patients allowed us to test the temporal dynamics of neocortical pattern reactivation, local neural oscillations (e.g., hippocampal ripples, cortical spindles), and hippocampal-cortical coupling. Based on recent TMR studies, we hypothesized that when auditory cues were presented during NREM sleep, some memories were selectively strengthened, and this was accompanied by specific signatures of reactivation, including hippocampal activation and hippocampal-cortical interactions.

Results

Experimental task and behavioral results

Eleven epilepsy patients (Table S1) participated in the object-location TMR paradigm (Fig. 1A, B, see section "Methods" for details). Briefly, participants learned to associate 50 unique items with specific locations on a grid, each item paired with a characteristic sound (e.g., goblet with breaking sound). After learning, a pre-sleep test was performed, during which participants had to place objects to the correct locations. During NREM sleep, the sounds for 25 objects were played in the expectation of causing a TMR effect[13]. When the participants woke up the next morning, all item locations were tested as in the pre-sleep test. Drop error was assessed as the Euclidean distance between the response location and the correct location. Drop error gradually decreased with the learning process (Fig. 1D): the drop error for the intermediate trials of learning phase was significantly lower than that for the first trial of learning phase ($t(10) = -7.665$, $p < 0.001$); the drop error for the last trial of learning phase was significantly lower than that for the intermediate trial of learning phase ($t(10) = -13.334$, $p < 0.001$). Critically, drop error for the pre-sleep test ($t(10) = -15.068$, $p < 0.001$) and the post-sleep test ($t(10) = -11.279$, $p < 0.001$) were significantly lower than the chance level, which indicated that the subjects carefully memorized the association between objects and locations. Drop error between cued and no-cued items in pre-sleep test was no significant difference (Fig. S1A). The measurement of memory change score was used to assess memory performance by comparing the accuracy of the recalled position in pre-sleep test and post-sleep test (see Methods for details). We found a significant though relatively weak TMR effect: memory change score was higher for objects cued by their sounds during sleep than for those not cued ($t(10) = 2.23$, $p = 0.049$ by paired-sample t-test; Fig. 1E). Further analysis showed that the variability in memory change due to TMR was not consistent for specific objects over subjects (Fig. S1C).
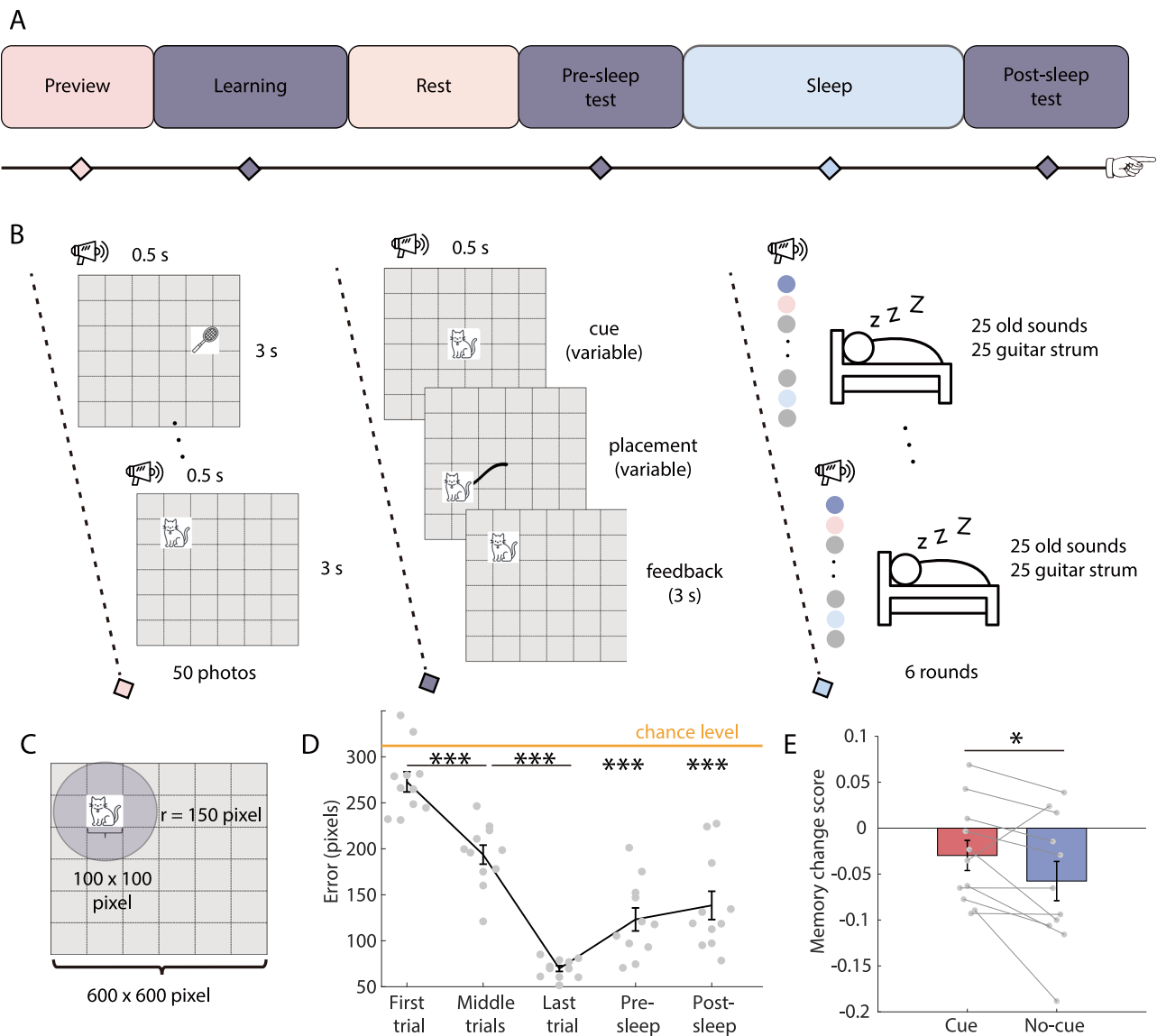
Fig. 1 | Task design and behavioral results. A experiment protocol. The experiment consisted of five consecutive stages: preview, learning, pre-sleep test, and post-sleep test. **B** Detailed task procedure. During preview phase (left), item paired with a characteristic sound was presented at specific locations one after the other and participants were instructed to remember the location of each item. In the learning stage (middle), trials started with an item presented in the center of the screen (also paired with a sound). Participants attempted to place each item to the correct location. After the participant confirmed item placement by a button press, the item was then displayed in the correct location as the feedback. The process of pre-sleep test and the post-sleep test were identical with learning except there was no feedback in the tests. During NREM sleep (right), the sounds for 25 items and 25 control sound (guitar strum) were played for six rounds. **C** The size of the item and the grid. Learning of items stopped once these items were placed within 150 pixels (circular area) surrounding the correct location on two consecutive rounds. **D** Drop error (mean values ± SEM) deceased with the learning process ($t(10) = -7.665$, $p < 0.001$; $t(10) = -13.334$, $p < 0.001$; from left to right, two-sided paired-sample t-test, $N = 11$) and was significantly lower than chance level during pre-sleep test, and post-sleep test ($t(10) = -15.068$, $p < 0.001$; $t(10) = -11.279$, $p < 0.001$; respectively, two-sided paired-sample t-test, $N = 11$). **E** TMR effect: memory change score (mean values ± SEM) were higher for objects cued by their sounds during sleep than for those not cued ($t(10) = 2.23$, $p = 0.049$ by two-sided paired-sample t-test, $N = 11$). The schematic illustrations (cat, racket, sleep and broadcast) are sourced from The Noun Project (https://thenounproject.com, icons created by Lewen Design, Maan Icons, Teewara soontorn and Ian Rahmadi Kurniawan, respectively) under a Royalty-Free License. *$p < 0.05$, ***$p < 0.001$.

Item-level cortical pattern around hippocampal ripples in learning stage

Cortical and hippocampal contacts for all subjects (Table S2) were separately shown in Fig. 2A, G. For each subject, one contact located in the hippocampus was selected for ripple detection (see "Methods" for details). The dataset included 7,763 ripples during the learning stage, corresponding to an average rate and standard deviation of 0.40 ± 0.14 events per second (ripple duration: 33 ± 12 ms), similar to the previous results[41]. In Table S4, we presented the distribution of ripple peak frequencies. It is worth noting that human ripple frequency is significantly lower than that of rodents[42–46], possibly due to the larger network involved in humans[47]. In addition, a detailed comparison of hippocampal ripples among various species by Buzsáki et al. revealed that the duration of human ripples was shorter than that of rodent ripples[48]. Liu et al. systematically summarized the characteristics and differences of ripples detection in rodent and primate[45]. Therefore, when detecting human ripples, we need to consider this species difference and carefully refer to the detection methods and results of
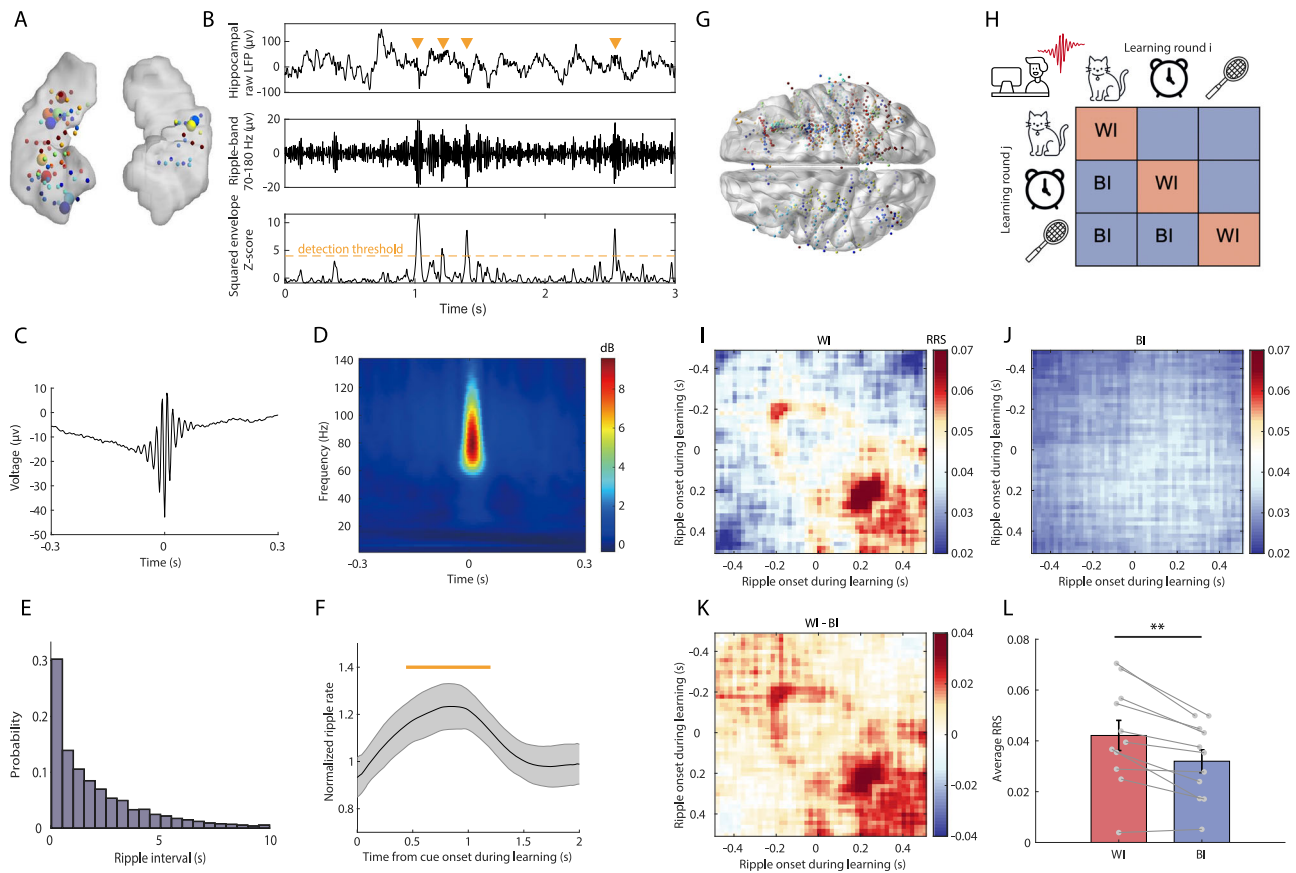
Fig. 2 | Item-level cortical high-gamma pattern around hippocampal ripples during the learning stage. A Depiction of hippocampal contacts in all patients ($N = 11$). Each color denotes one patient, and for each participant, we select one hippocampal contact to identify ripples (marked by large spheres). **B** Example of ripple events in hippocampal recordings during the learning stage. From top to bottom: raw hippocampal LFP; ripple-band filtered LFP (70–180 Hz); normalized ripple-band envelope above the threshold were detected as ripple events. **C, D** Grand average peri-ripple field potential and spectrogram during learning phase ($n = 7763$ ripple events from 11 patients). **E** Distribution of inter-ripple intervals. **F** Normalized ripple rate (mean values ± SEM) triggered by cue onset during the learning stage. The yellow bar indicates time period of significant increases in ripple rate ($p = 0.032$, cluster-based permutation test based on one-sided paired-sample t-test, $N = 11$). **G** Distribution of all intracranial cortical contacts

in all patients ($N = 11$). **H** RRS (retrieval-retrieval similarity) schematic illustration between different learning rounds. Cortical activity pattern around ripple onset (±500 ms) was correlated either between trials with the same items (WI) or between different items (BI). Item-level representation was calculated by subtracting BI similarity from WI similarity. **I** Averaged WI similarity. **J** Averaged BI similarity. **K** Averaged Item-level representation. **L** WI similarity (averaged across ±0.5 s) was significantly higher than BI similarity ($t(10) = 4.54$, $p = 0.001$, two-sided paired-sample t-test, $N = 11$). Data are presented as mean values ± SEM. **p < 0.01, RRS: difference of retrieval-retrieval similarity. WI within item. BI between item. The schematic illustrations (clock and computer) are sourced from The Noun Project (https://thenounproject.com, icons created by Thea Graph and Maxicons, respectively) under a Royalty-Free License.

previous human studies. Our results showed that the frequency and duration of ripples detected in the present study were consistent with findings reported in previous human ripple studies[26,41]. Distributions of between-ripple intervals, grand-average peri-ripple field potential and spectral decomposition of ripples during the learning were shown in Fig. 2B–E. The ripple occurrence rate of each subject is shown in Table S3.

We normalized ripple rate within subject to account for individual variation in ripple rate (see section "Methods" for details). Then we examined whether ripples occurred during a specific time during retrieval phase. We assessed ripple rate 0-2000 ms after stimulus onset and observed that the normalized ripple rate between 440–1200 ms (Fig. 2F) after stimulus onset was significantly higher than baseline ($p = 0.032$, cluster-based permutation test). To further investigate whether the ripple rate during learning was associated with successful recall of item location, we divided the learning trials into two groups based on the drop error in either the pre-sleep or post-sleep test (Fig. S2A). The results revealed that the ripple rate in the low error group was significantly higher than that in the high error group.

Previous studies indicated that ripples played an important role in the reactivation of mnemonic information[3,41,49]. We further investigated whether item level representations can be detected around the occurrence of ripple during retrieval phase. We applied Spearman correlation to assess the retrieval-retrieval neural pattern similarity (RRS) in high-gamma band (50–140 Hz). Within-Item (WI) similarity was calculated as the cortical pattern similarity between trial pairs with the same item (Fig. 2I), while Between-Items (BI) similarity was calculated as the cortical pattern similarity between trial pairs with different items (Fig. 2J). The item-level neural representation was determined by observing significantly greater WI similarity compared to BI similarity (Fig. 2K, L). Our analysis revealed significant item-level neural representations ($t(10) = 4.54$, $p = 0.001$). This indicated that the cortical high-gamma patterns around hippocampal ripple contained item-level information. To test the hypothesis that the representation was item-specific or influenced by memory effects, we divided the items into two groups based on the drop error of the pre-sleep test or memory change scores, and then calculated the respective item-specific representations (WI-BI) for each group (Fig. S3). All subgroups showed significant differences from zero, but no significant difference

was observed between the subgroups. This indicated that item-specific representations were not linked to memory effects.

Two behavioral-relevant item reactivations during sleep

Previous researchers have identified the reactivation of corresponding objects (categories) during sleep after TMR-cues are played[17,20,50]. We aimed to investigate whether the reactivation induced by auditory cues during sleep heterogeneously affected memory consolidation of specific items. Firstly, we computed the Retrieval-Sleep Similarity (RSS) by calculating Spearman correlation between the cortical high-gamma patterns during learning ripples and patterns during sleep after corresponding TMR cue onset (Fig. 3A, Step 1). The gamma pattern is a vector (1 × contacts) composed of gamma power (averaged from 50 to 140 Hz) of every cortical contact. Subsequently, we assessed the Spearman correlation between RSS and memory change scores for each subject and each round (Fig. 3A, Step 2). The averages across subjects and rounds were depicted in Fig. 3B. After the cluster-based permutation test, two significant clusters emerged (Fig. 3B, $p = 0.004$, $p = 0.003$, from left to right; Fig. 3C). We compressed the Y-axis of Rho matrix to more clearly display the dynamic changes in reactivation (Fig. S4A). To rule out the effect of sound stimulus durations on reactivation patterns, we realigned the representational similarity data of each trial to the offset of the sound stimulus. We then recalculated the correlation between RSS and memory change scores (Fig. S5). Similar to Fig. 3B, we still found two significant clusters. To validate the stability of this behavioral-relevant reactivation pattern, we calculated this pattern for each round (Fig. S6) and each subject (Fig. S8), and accessed the similarity between this pattern for each round (Fig. S7) and each subject (Fig. S9) with the pattern of the main result. Overall, our results indicated a notably stable behavioral-relevant item reactivations pattern (for both round level and subject level, $p < 0.001$ with Binomial test). In addition, to further verify whether multiple reactivations occurred individually, we extracted the oscillatory components[51] from the behavioral-relevant reactivation matrix and observed strong low-frequency oscillations for each subject, with an average frequency peak of 0.8 Hz (Fig. S10). This indicated that multiple reactivations indeed occurred at the subject level.

To further validate the robustness of behavioral-relevant reactivation, we applied a different ripple detection criterion (filtering in 80–120 Hz and at least 3 cycles) across all hippocampal contacts. We then recalculated the reactivation, as shown in Fig. S11. There were three significant reactivation clusters (cluster1: from 400 ms to 1320 ms, $p = 0.006$; cluster2: from 2010 ms to 2460 ms, $p = 0.008$; cluster3: from 2840 ms to 3740 ms, $p = 0.004$; from left to right), with the second and third reactivation clusters aligning with our main results. We also verified that the timing of reactivation on the Y-axis does not show a significant difference from the main results (Fig. S11D, E). In addition, a significant reactivation cluster emerged around 1-s post cue, which was consistent with previous research suggesting that reactivation directly after TMR may be driven by sensory stimuli[12].

In order to investigate the neural mechanisms underlying consolidation selectively benefits for some items, we split the 25 cued items into memory strengthening group and memory decaying group (i.e., the top group with the strongest memory change score (9 items) was categorized into a "strengthening" condition and the bottom group with the lowest score (9 items) into a "decaying" condition) (Fig. 4A). No significant difference between strengthening and decaying items was found in hippocampal ripple rate during learning (Fig. S2B). However, we found that reactivation was significantly higher for items from the memory-strengthening condition than for those from the memory-decaying condition during two temporal clusters (Fig. 4B, Cluster 1: 1.6–2.6 s, $p = 0.018$; Cluster 2: 2.8–3.8 s, $p = 0.020$; cluster-based permutation test). We compressed the Y-axis of RSS matrix to more clearly display the dynamic changes in reactivation (Fig. S4B). We also conducted two control analyses to verify the

specificity of the reactivation pattern by using non-learning-ripple trials data and control condition (guitar strum) data (Fig. S12). The difference between strengthening and decaying items of non-ripple trials showed a similar trend as ripple trials did (Fig. S12A, minimum P-value = 0.056, cluster-based permutation test). In addition, we tested whether the reactivation results were driven by differences in pre-sleep accuracy of strengthening vs. decaying items ($t(10) = 7.3$, $p < 0.001$; Fig. S1B), and compared reactivation of two groups of items determined entirely by pre-sleep accuracy but matched for memory change score. RSS results showed no significant reactivation differences between the two groups (Fig. S13), indicating that higher reactivation of strengthening items cannot be purely explained by differences in pre-sleep accuracy.

Differential occurrence rate of hippocampal ripples and cortical spindles during two reactivations

We further investigated the temporal dynamics of neural oscillations during the TMR period. We first detected hippocampal ripples and cortical spindles during sleep (Fig. 4C–E). The results showed that there were indeed hippocampal ripples and cortical spindles occurring in this period (Fig. S14). Subsequently, we compared the ripple and spindle rate differences using repeated measures ANOVA between the three conditions (strengthening, decaying and control) during the two intervals (1.6–2.6 s and 2.8–3.8 s). During the first reactivation, the repeated measures ANOVA revealed a significant difference between the ripple rate for the three conditions ($F_{(2,20)} = 3.7$, $p = 0.043$). Post-hoc t-tests showed that the ripple rate of the strengthening condition was significantly higher than that of control conditions ($t(10) = 2.31$, $p = 0.043$), and showed an increasing trend than that of the decaying conditions, but did not reach statistical significance ($t(10) = 2.174$, $p = 0.054$). However, during the second reactivation, there was no significant difference among the three conditions ($F_{(2,20)} = 0.21$, $p = 0.81$, Fig. 4F). Concerning cortical spindles, no differences were observed between the three conditions during the first reactivation ($F_{(2,20)} = 0$, $p = 0.998$). During the second reactivation, the repeated measures ANOVA revealed a significant difference between the three conditions ($F_{(2,20)} = 5.58$, $p = 0.012$). Post-hoc t-tests showed that the strengthening condition exhibited a significantly higher spindle rate than the decaying and control conditions ($t(10) = 2.637$, $p = 0.025$; $t(10) = 3.226$, $p = 0.009$, respectively, Fig. 4G).

In addition, time-frequency spectrograms of hippocampus and cortex during these two intervals also supported the above findings from another perspective. There were significant clusters in the frequency range of ripples in the hippocampus only during the first reactivation (Fig. S15B, $p < 0.01$, cluster-based permutation test). When comparing cortical spectrograms between the two conditions, we found difference in spindle activity during the first reactivation period. But it should be pointed out that the intensity of the difference was lower than the subsequent second reactivation cluster. This result suggests that the changing trend of spindle activity differences (strengthening>decaying) is consistent with the result of spindle events detection (Fig. S15A, $p < 0.01$, cluster-based permutation test). The findings indicated that the two sequential reactivations separately associated with hippocampal oscillations (increased ripples) and cortical oscillations (increased spindles) may be indicative of distinct roles in memory consolidation.

Dynamic hippocampal-cortical synchronization during two reactivations

We calculated hippocampal-cortical coherence to measure inter-regional synchronization during time periods of two reactivations. As shown in Fig. 5A, coherence was significantly enhanced for strengthening over decaying items and control condition during the first reactivation (frequency range $_{strengthening > decaying}$, 16–30 Hz: $p < 0.001$; frequency range $_{strengthening > control}$, 20–45 Hz: $p < 0.001$;
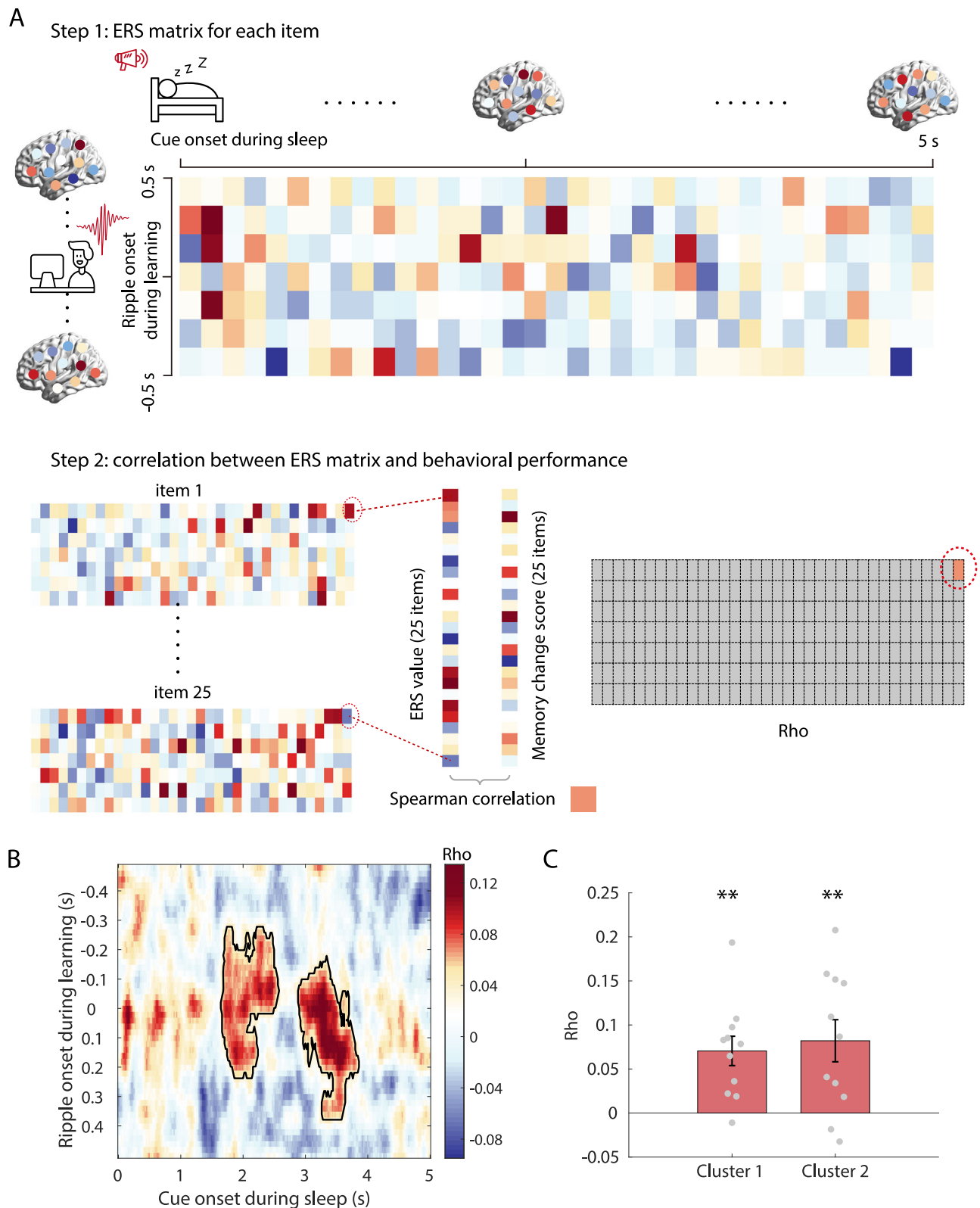
Fig. 3 | Behavioral-relevant item reactivations during sleep. A Procedure for calculating behavioral-relevant item reactivations. Step 1: computing the Retrieval-Sleep Similarity (RSS) between the cortical high-gamma patterns around ripple onset during learning and the corresponding patterns during sleep after cue onset for each item. The gamma pattern is a vector (1 × contacts) composed of gamma power (averaged from 50 to 140 Hz) of every cortical contact. Step 2: calculating the Spearman correlation (Rho) between RSS and memory change scores over 25 items. **B** The average Rho across subjects and rounds. Two significant clusters emerged after the one-sided cluster-based permutation test ($p = 0.004$, $p = 0.003$, from left to right, $N = 11$). **C** The average Rho within Cluster 1 and Cluster 2 are both significantly greater than zero ($t(10) = 4.26$, $p = 0.002$, $t(10) = 3.44$, $p = 0.006$, $N = 11$, one-sided paired-sample t-test and Bonferroni correction, from left to right, respectively). Data are presented as mean values ± SEM. **p < 0.01. The schematic illustrations are sourced from The Noun Project under a Royalty-Free License.
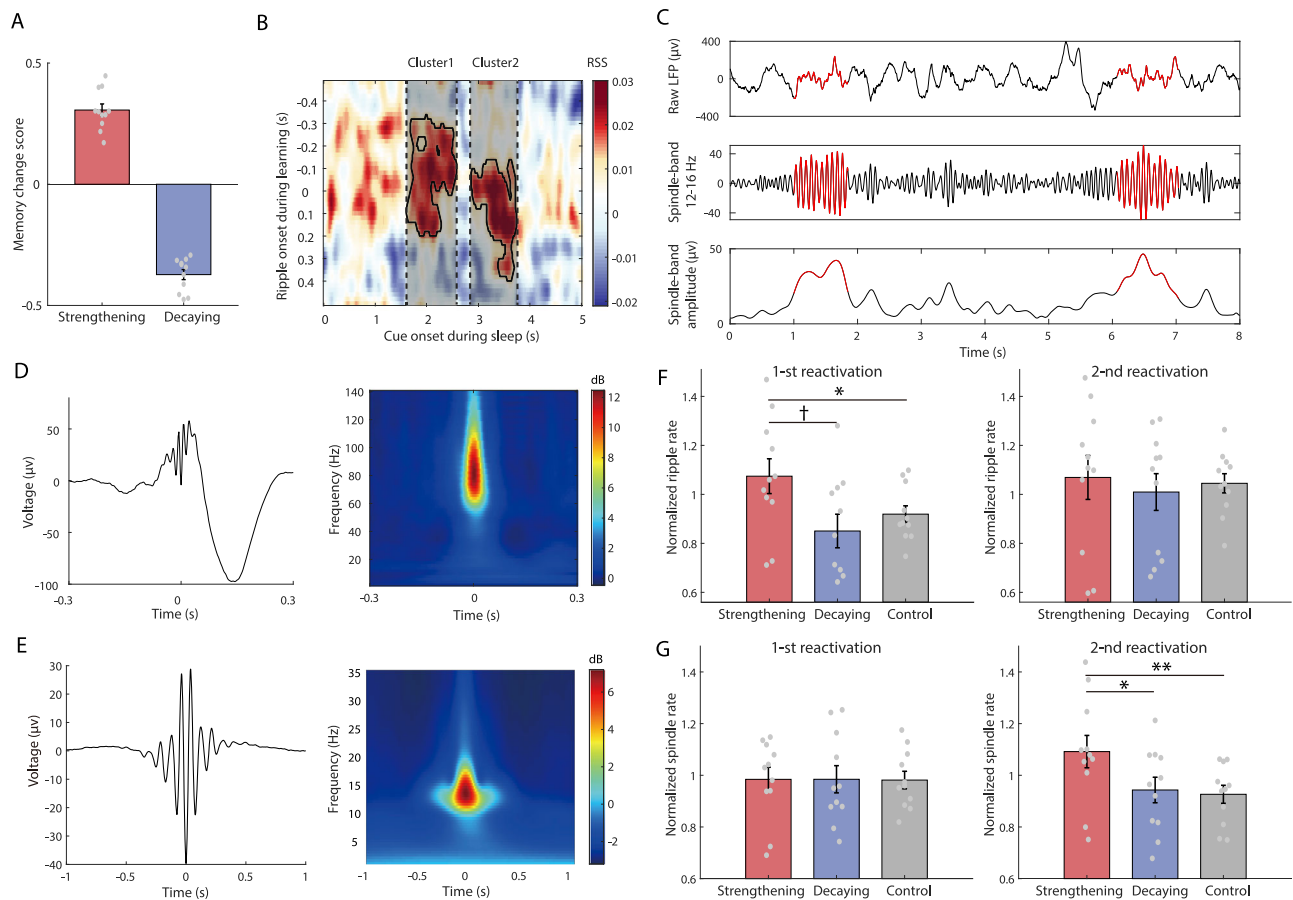
Fig. 4 | Different ripple and spindle patterns during two reactivations.
A Memory change score (mean values ± SEM) in the memory strengthening condition (red) and the memory decaying condition (blue), $N = 11$. **B** The heat map shows the difference of reactivation (RSS, difference of retrieval-sleep similarity) between strengthening and decaying items averaged across patients ($N = 11$). Two temporal clusters (outlined in black, i.e., two shaded areas) survived after cluster-based permutation test based on one-sided paired-sample t-test ($p = 0.018$, $p = 0.020$, from left to right, respectively). **C** Example of detected spindle events in cortical recordings during sleep. From top to bottom: raw cortical LFP; spindle-band filtered LFP (12–16 Hz); spindle-band envelope used for spindle detection. **D** Grand average peri-ripple field potential (left) and spectrogram (right) during sleep ($n = 6991$ ripple events from 11 patients). **E** Grand average peri-spindle field

potential (left) and spectrogram (right) during sleep ($n = 69,947$ spindle events from 11 patients). **F** Hippocampal ripple rate (mean values ± SEM) of the strengthening condition is significantly higher than that of the control conditions ($t(10) = 2.31$, $p = 0.043$, two-sided paired-sample t-test, $N = 11$) and showed an increasing trend than that of the decaying conditions, but did not reach statistical significance ($t(10) = 2.174$, $p = 0.054$, two-sided paired-sample t-test, $N = 11$) during the first reactivation (left), but not the second reactivation (right). **G** Cortical spindle rate (mean values ± SEM) of the strengthening condition is significantly higher than that of the decaying and control conditions during the second reactivation ($t(10) = 2.637$, $p = 0.025$; $t(10) = 3.226$, $p = 0.009$, respectively, two-sided paired-sample t-test, $N = 11$), but not the first reactivation (left). $†p < 0.1$, $*p < 0.05$, $**p < 0.01$.

cluster-based permutation test). This result was reversed during the second reactivation (Fig. 5E; frequency range $_{decaying > strengthening}$, 10–21 Hz: $p = 0.001$; frequency range $_{decaying > control}$, 10–21 Hz: $p < 0.001$, cluster-based permutation test). We used imaginary coherence to obtain similar results, thereby ruling out the influence of volume conduction effects (Fig. S16). We further found the hippocampal-cortical coherence was mostly contributed by the ipsilateral recording sites (Fig. S17). In a complementary analysis, we assessed the time-resolved coherence by averaging coherence of the strengthening condition across the frequency range 16–45 Hz (the union of frequency range $_{strengthening > decaying}$ and frequency range $_{strengthening > control}$; Fig. S18A). We found significant differences between the two reactivation periods (Fig. S18B). Given that cortical pattern reactivation was stronger for strengthening items during both intervals, the reversed effect of hippocampal-cortical connectivity may reflect beneficial effects of early coupling and subsequent decoupling between hippocampus and cortical areas.

Previous research suggested that both cortical ripples and HFB signals coupled to the hippocampal ripple events can reflect hippocampal-cortical information communication[24,26,27]. Therefore, in

order to further investigate the hippocampal-cortical interaction, we tested whether cortical HFB activities were coupled with hippocampal ripples during the two reactivations. The repeated measures ANOVA indicated a significant difference between three conditions ($F_{(2,3276)} = 47.858$, $p < 0.001$) during the first reactivation. Post-hoc t-tests revealed that differences between two conditions were significant in the three conditions (LME $_{strengthening\ vs.\ decaying}$, $t(1092) = 9.064$, $p < 0.001$; LME $_{strengthening\ vs.\ control}$ $t(1092) = 5.943$, $p < 0.001$; LME $_{decaying\ vs.\ control}$ $t(1092) = -4.909$, $p < 0.001$; Fig. 5B). Given that cortical-hippocampal coherence was notably enhanced during the first reactivation, we further investigated the relationship between coherence and cortical HFB coupled with the hippocampal ripple. For this purpose, we selected contacts that showed coherence above the median level for each subject. We then calculated the correlation between the hippocampal ripple-coupled-HFB power and the coherence (16-30 Hz) within each subject. Notably, the intensity of the HFB power was positively correlated with hippocampal-cortical coherence ($t(10) = 3.02$, $p = 0.013$, Fig. 5C; an example as in Fig. 5D). In addition, coupled ripples between hippocampus and cortex were more pronounced in strengthening items than decaying items during
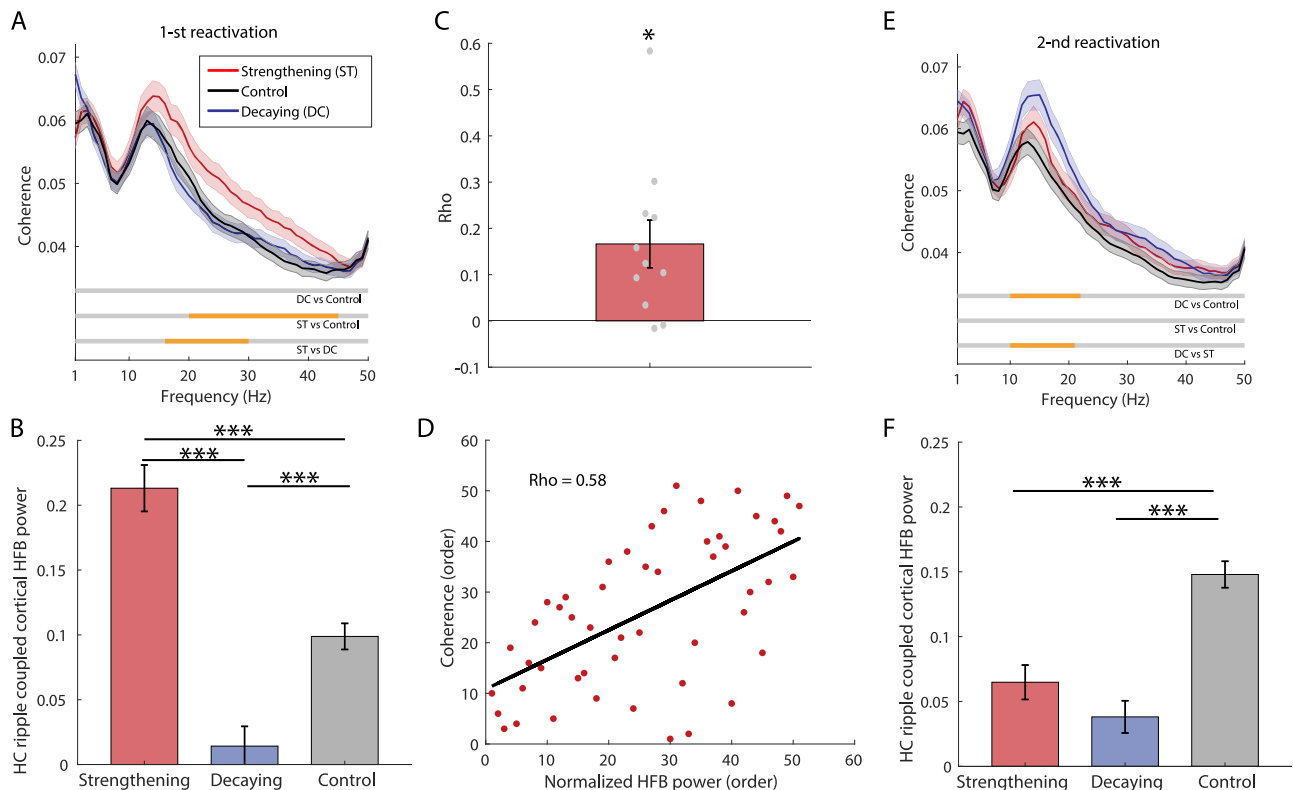
Fig. 5 | Dynamic hippocampal-cortical synchronization during two reactivations. A Coherence (mean values ± SEM) between cortex and hippocampus is significantly (yellow lines marked) enhanced for strengthening over decaying items (16–30 Hz) and control condition (20–45 Hz) during the first reactivation ($p < 0.001$; cluster-based permutation test based on two-sided LME, $N = 1093$ contacts). **B** Hippocampal ripples coupled with cortical HFB (mean values ± SEM) in the strengthening condition are significantly stronger than that in both the decaying and control conditions during the first reactivation (two-sided LME $_{strengthening\ vs.\ decaying}$: $t(1092) = 9.064$, $p < 0.001$; two-sided LME $_{strengthening\ vs.\ control}$: $t(1092) = 5.943$, $p < 0.001$; two-sided LME $_{decaying\ vs.\ control}$ $t(1092) = -4.909$, $p < 0.001$; $N = 1093$ contacts). **C** Significant positive correlation between hippocampal-cortical coherence (16–30 Hz) and hippocampal-ripples coupled cortical HFB ($t(10) = 3.02$, $p = 0.013$, two-sided paired-sample t-test, $N = 11$). Data are

presented as mean values ± SEM. **D** An example subject shows a positive correlation between hippocampal-cortical coherence and hippocampal-ripples coupled cortical HFB. **E** hippocampal-cortical coherence (mean values ± SEM) is significantly (yellow lines marked) enhanced for decaying than strengthening items (10–21 Hz) and control condition (10–21 Hz) during the second reactivation ($p < 0.001$; cluster-based permutation test based on two-sided LME, $N = 1093$ contacts). **F** Hippocampal ripples coupled with cortical HFB (mean values ± SEM) in the strengthening and decaying condition are significantly weaker than that in the control conditions during the second reactivation (two-sided LME $_{control\ vs.\ strengthening}$, $t(1092) = 5.394$, $p < 0.001$; two-sided LME $_{control\ vs.\ decaying}$, $t(1092) = 7.771$, $p < 0.001$; $N = 1093$ contacts). HC hippocampus. *$p < 0.05$, ***$p < 0.001$.

the first reactivation (LME $_{strengthening\ vs.\ decaying}$, $t(596) = 4.632$, $p < 0.001$, Fig. S19). During the second reactivation, the repeated measures ANOVA indicated a significant difference between three conditions ($F_{(2,3276)} = 25.498$, $p < 0.001$). Post-hoc t-tests revealed that the HFB power in the control condition was significantly higher as compared to the strengthening condition and decaying condition (LME $_{control\ vs.\ strengthening}$, $t(1092) = 5.394$, $p < 0.001$; LME $_{control\ vs. decaying}$, $t(1092) = 7.771$, $p < 0.001$). There is no significant difference between strengthening condition and decaying condition (LME $_{strengthening\ vs.\ decaying}$, $t(1092) = 1.536$, $p = 0.125$; Fig. 5F). The above results suggested that for selectively enhanced memories, hippocampal-cortical communication significantly increased during the first reactivation, but significantly decreased during the subsequent reactivation.

In sum, TMR cues played during NREM sleep may enable selective memory consolidation through alternating periods of coupling and decoupling between cortex and hippocampus. Firstly, the hippocampus communicated with the cortex through coherence and coupled neural oscillations (ripples & HFB). After that, the cortex and hippocampus were decoupled, while cortical processing may proceed independently, manifested by enhanced cortical spindle activity. Based on the above results, we propose a dynamic model for memory consolidation after TMR cues during NREM sleep (Fig. 6).

Discussion

This study showed that arbitrarily selected sound cues presented during sleep did not uniformly impact memory storage, as there was relative strengthening and decaying. Importantly, there were significant differences in neurophysiological responses between strengthening and decaying memories, even though both types were cued the same number of times during NREM sleep. The memory-strengthening items showed (a) stronger cortical reactivations in two consecutive windows, (b) increased hippocampal ripple activity (ripple rate & ripple-band power) during the first reactivation, and (c) increased cortical spindle activity (spindle rate & spindle power) during the second reactivation. Results revealed a complex temporal dynamic between local processing (i.e., hippocampal ripples, cortical pattern reactivation, cortical spindle activity, and cortical HFB) and inter-regional interaction (i.e., hippocampal-cortical coupling).

Representation similarity analysis, as applied here, provides a powerful way to probe the relationship between cortical reactivation and memory enhancement. Our results showed that cortical reactivation differed between strengthening memories and decaying memories in ways that we interpret as reflecting additional processing that supports consolidation. Memory reactivation (or "replay") has long been considered in connection with post-acquisition facilitation of memory storage[16,17,19,20]. Furthermore, our study revealed multiple

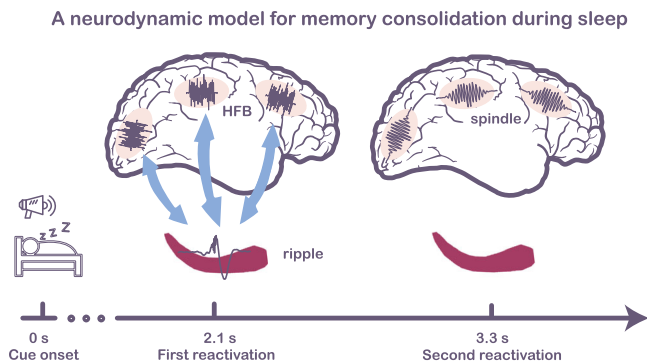### A neurodynamic model for memory consolidation during sleep

Fig. 6 | A neurodynamic model for selective memory consolidation during sleep. After TMR cue onset, we observed two consecutive time periods with significant cortical pattern reactivation. Hippocampal ripple rate significantly increases during the first reactivation. Meanwhile, there exists stronger hippocampal-cortical interaction, including hippocampal-cortical coherence and co-occurrence of hippocampal ripple and cortical HFB activity. During the second reactivation, the cortex and hippocampus is decoupled, perhaps allowing cortical processing to proceed independently, manifested by enhanced cortical spindle activity. Note that the cortical positions shown in Fig. 6 are only for illustration purposes. HFB: high-frequency broadband. TMR: targeted memory reactivation. Note. Schematic brain reprinted from scidraw.io (Chilton, J. (2020). Brain outline. Zenodo. https://doi.org/10.5281/zenodo.3925989). CC BY.

TMR-induced memory reactivations. This result suggests that memory consolidation during NREM sleep may require multiple reactivations. Until now, few studies have explored this hypothesis. Bendor and Wilson trained rats in an auditory-spatial association task and found that sound cues during slow-wave sleep induced reactivation of hippocampal place cells. Such cue-evoked hippocampal reactivation lasted for 10 s, until the next acoustic cue appeared[19]. Human electrophysiological studies have also produced evidence that memory reactivation triggered by TMR stimulation occurs more than once[20]. Based on these findings, it has been proposed that memory enhancement depends on the "echoing" of memory information in the hippocampal-cortical loop[12]. A recent work found that spindle-locked ripples in MTL were tightly related to the memory reactivation during human NREM sleep[52]. However, they mainly focused on the early reactivation after TMR cue (within 1.5 s), and did not investigate the information interaction between the hippocampus and cortex during memory reactivation.

Our study revealed a complex relationship between hippocampal ripples and cortical pattern reactivation. Many previous researches have argued that hippocampal ripples play an important role in memory consolidation[21,22,53,54]. Previous literature suggests that hippocampal ripples are associated with reactivation of mnemonic information and information transmission between hippocampus and cortex[21,24,25]. Disrupting sharp-wave ripples in the rat hippocampus by electrical stimulation during post-training periods significantly impairs spatial memory[55]. Our study found no difference in ripple rate between wakefulness and NREM sleep, consistent with the findings in recent studies[3,56]. However, other studies also reported significant differences in ripple rate between two states[57,58]. This suggests that the difference in ripple rate between wakefulness and NREM sleep remains inconclusive and requires further clarification in future studies. Human electrophysiological studies have also confirmed that hippocampal ripples and ripple-related reactivation during NREM sleep are associated with post-sleep memory performance[3,59]. In addition, some researchers found that hippocampal ripples and cortical reactivation tend to occur closely in time[41,49,60–63]. However, considering the echoing effect of TMR-induced reactivation, these previous studies have not indicated whether there are hippocampal ripples during the

multiple cortical reactivation periods after TMR cue. The present study found robust hippocampal ripples and cortical spindles occurring in the two cortical reactivations. The ripple rate of the strengthening condition was significantly higher than that of the decaying and control conditions during the first reactivation but not the second reactivation. Interestingly, cortical spindles exhibited the opposite tendency. The spindle rate of the strengthening condition was significantly higher than that of the decaying and control conditions during the second reactivation but not the first reactivation. In addition, the time-frequency analysis found similar trends with the spindle detection analysis. The spindle activity differences (strengthening>decaying) during the first reactivation were obviously lower than the subsequent second reactivation. The results indirectly support the theoretical explanation of reactivation induced by TMR[12]. TMR-induced memory enhancement may necessitate that the hippocampus first replays and transmits memory information to cortex in the form of ripple messages. Subsequent cortical reactivation may represent complete and independent replay of those memories.

The second core finding of the present study concerned the complex temporal dynamics of coupling between hippocampus and cortex. Compared with decaying memories, strengthening memories showed stronger hippocampal-cortical coupling during the first reactivation, an effect that reversed during the second reactivation. In other words, the degree of coherence for strengthening memories actually decreased from the first reactivation to the second reactivation. Previous studies have found that TMR can significantly enhance hippocampal-cortical functional connectivity[33–35]. However, due to the limited temporal resolution of fMRI, it remains unclear how hippocampal-cortical connectivity changes when cortical reactivation occurs. The present study showed that the hippocampal-cortical coupling during memory reactivations is not constant and exhibit complex temporal dynamic. More noteworthy was that during the first reactivation period, cortical HFB and ripples coupled to hippocampal ripples in the strengthening condition was significantly stronger than that in the decaying condition, and it was positively correlated with the degree of hippocampal cortical coupling. Both cortical ripples and high-frequency broadband signal coupled to the hippocampal ripple events can reflect hippocampal-cortical information communication[24,26,27]. This discovery may be consistent with some assumptions of the system consolidation theory. This theory hypothesized that newly encoded memories are initially distributed in the hippocampus and cortex[22,64,65]. Subsequently, in NREM sleep, the new memory needs to be transformed into a stable long-lasting memory through hippocampal-cortical interactions. The hippocampus may play a key role in integrating initial memory information, and transmitting the integrated memory to the cortex[1,12,22,31]. It is worth noting that coupling between hippocampus and cortex not only exists in periodic oscillations (e.g., spindle), but also covers broadband activities (e.g., 16–45 Hz). This may suggest the potential value of aperiodic activities in memory consolidation during sleep. Previous studies have suggested that aperiodic activities have different characteristics from periodic oscillations during both wake and sleep periods[66–69]. Therefore, in future research, we can attempt to investigate the characteristics of aperiodic neural activities during sleep memory consolidation process.

According to the above theoretical viewpoints and our empirical results, we proposed the following multi-part scenario. During the first reactivation, (i) strengthening memories showed more pronounced hippocampal-cortical coupling and cortical HFB activities coupled to hippocampal ripples, may imply associations between hippocampus and cortex during memory reactivation. Then, (ii) hippocampal processing led to integration of the components of the item-location association, including the context of that learning, (iii) as manifested by hippocampal ripples. During the second reactivation, (iv) hippocampal-cortical coupling decreased. At the same time, local spindle band activity

in cortex increased, (v) maintaining and strengthening the cortical representations. That is, the hippocampus may have completed information integration and transmission during the first reactivation; subsequently, there was no need for further hippocampal information transmission, as the cortical representation was replayed independently in the service of improving long-lasting storage.

Importantly, behavioral analysis showed that TMR benefits were more apparent for items with low pre-sleep accuracy. The performance difference before sleep could be one driving force for later effects during sleep. Previous TMR studies have produced similar results[36,37], and this effect may have multiple causes. One factor likely is that enhanced accuracy after sleep in those trials may reflect regression to the mean. Correspondingly, reduced accuracy after sleep for trials with high pre-sleep accuracy could also reflect regression to the mean, indicating that the memory differences between the two critical conditions could entirely reflect measurement variability. However, this factor cannot account for the present results because neural correlates of memory change would not be expected if memory change was due merely to such unsystematic fluctuations in performance. Another factor described in prior studies is that gains from TMR tend to be more apparent for weak memories than for strong memories[36,70]. Notably, the control analysis showed that though two groups of trials showed significant differences in test accuracy at the pre-sleep stage, we did not find a significant reactivation difference if the two groups did not differ in memory change (Fig. S13). The evidence thus indicates that the reactivations during TMR period supported selective memory consolidation process. The above control analysis excluded its relationship with pre-sleep memory accuracy. It is worth noting that although iEEG recording in epilepsy patients does provide rare opportunity to directly measure neurophysiological responses. As widely understood, it is not possible to directly compare iEEG results in those with versus without epilepsy due to the inability to record the same intracranial EEG data from healthy individuals. Therefore, the possibility that the results could be influenced by changes in the epileptic brain cannot be ruled out. Therefore, when generalizing the conclusions of the present study, we should be careful of this limitation.

For intracranial EEG recording, there are differences in the number and position of electrodes for each subject, which limits the stability of RSA analysis (especially for item-level similarity analysis). In addition, when conducting experiments in the bedside, it is difficult to control factors such as the sleep stages (NREM 1–3) on which the TMR cues were delivered and the phases (up/down states) of the SO on which the TMR cues were delivered. Considering the limitations, in future, we will use more sophisticated recording method (such as single-neuron recording) and close-loop TMR intervention to test the stability of multiple reactivations phenomena. Furthermore, the coupling of slow waves, spindle, and hippocampal ripples plays an important role in memory consolidation. In our data, we observed a clear coupling between these three oscillatory events during TMR (Fig. S21). However, due to the low incidence of coupling events (Table S5), it was difficult to analyze the triple-coupling contribution to memory effects. To precisely test this question, future studies may reduce the amount of items and increase the number of trials.

In sum, our findings suggest that cortical reactivation and hippocampal-cortical interactions support memory enhancement. A complex temporal dynamic between hippocampus and cortex manifested in neural patterns during NREM sleep in our study. Firstly, the hippocampus integrated and transmitted information with the cortex through functional connectivity and coupled neural oscillations, and then the cortex independently processed memory representations to support long-lasting memory storage.

Methods
Participants
Eleven patients (2 females and 9 males; mean age ± standard deviation (SD): 23.9 ± 5.4 years) with medically refractory temporal lobe epilepsy were recruited in the current study at Beijing Sanbo brain hospital. They voluntarily participated in this study without compensation. They were stereotactically implanted with depth contacts to identify epileptogenic zones. Demographic information for each patient is shown in Table S1. All patients reported normal or corrected-to-normal visual acuity and normal color vision. Informed consent was obtained from all participants and study procedures were approved by the ethical committee of Beijing Sanbo brain hospital.

Experimental task
We used an object-location association task adapted from that used in prior TMR studies[13,33,34]. Participants learned to associate each of 50 unique objects (small squares with a side length of 2.3 cm) with a specific location on a grid displayed on a monitor (13.6 cm square). At the same time, each object was paired with a characteristic sound (e.g., goblet with breaking sound). The experiment consisted of five consecutive stages: preview, learning, pre-sleep test, sleep, and post-sleep test. The preview stage was to ensure that the subjects understood the experimental instruction and the unique locations of each object. In the learning stage (including study and retrieval phase), participants attempted to place each object in the correct location (i.e., retrieval phase). Trials were self-paced and terminated after the participant confirmed object placement by a button press. The object was then displayed in the correct location for 3000 ms as the feedback (i.e., study phase). Following the procedures in a previous study[13], participants completed several rounds of learning with items in random order until all objects were placed within 3.4 cm of the correct location on two consecutive rounds. If an object was placed correctly on two consecutive rounds, it did not appear in the subsequent round. Approximately 40 min after the learning stage, during which time participants were allowed to rest, the pre-sleep test was administered with all 50 objects and no feedback, providing pre-sleep memory results.

After this test, participants went to sleep. The experimenter turned off the lights and played white noise at a low intensity (~55 dB sound-pressure level) from a Bluetooth speaker placed ~0.5 m from the participant's head. When the participant entered the first NREM stage 2 or 3 (detected using scalp EEG, see below), a randomized stimulus sequence including 25 old cued sounds and 25 new standard sounds (all guitar strum) was presented. The 25 cued sounds presented during NREM sleep were randomly chosen for each participant with the requirement that pre-sleep test accuracy was matched for cued and un-cued objects (all $p > 0.8$). The interval between two sound onsets was about 5.5 s. Each sound stimulus was presented 6 times (total TMR stimulation time about 30 min) during NREM sleep (for the first two participants in Table S3, the cued sound stimuli were played 3 and 4 times, respectively). When the participants woke up the next morning, all object locations were tested as in the pre-sleep test. The average time spent by participants in the experiment as follows: learning, 29.9 ± 9.4 minutes; pre-test, 5.9 ± 0.6 min; post-test, 5.8 ± 1.1 min.

Electrophysiological recordings
The surgical implantation of electrodes was performed purely based on clinical demands. Intracerebral multiple-contact electrodes (8–16 contacts; length: 2 mm, diameter: 0.8 mm, distance 1.5 mm; Huake-Hengsheng Medical Technology Co. Ltd, Beijing, China) were implanted with a robot-assisted stereotactic surgery system. Intracranial EEG and polysomnographic recordings were obtained with a Nicolet system (128 channels, sampling rate: 512 Hz; Thermo Nicolet Corporation). No seizure occurred during the task period and sleep. All data analysis was performed in MATLAB (MathWorks Inc., Natick, MA) using EEGLAB[71], Fieldtrip[72], analysis scripts published in previous studies[41,73] as well as custom-developed scripts in this study.

Intracranial electrode localization

To determine the exact anatomical placement of the electrodes, post-implantation CT images were co-registered to pre-operative T1-weighted MR images using FreeSurfer (v6.0.0, http://surfer.nmr.mgh.harvard.edu/). We reconstructed the implanted electrodes using previously published localization software[74] and visually verified the accuracy of electrode contacts localization. Then, all coordinates were mapped into Montreal Neurological Institute (MNI) standard space. The exact contact locations in the hippocampus were identified anatomically in each patient using FreeSurfer's parcellation algorithm[75] and ascertained by visual inspection.

IEEG data preprocessing

Similar to a previous study[3], we re-referenced all iEEG data (except for hippocampal contacts) by the average activity across all contacts, to optimize the specificity of representational patterns at individual contacts. For each hippocampal contact, a reference signal from a nearby white-matter contact was subtracted to eliminate common noise[41]. For each participant, we extracted data during the learning stage and during the TMR stage (10 s before the first stimulus to 10 seconds after the last stimulus). Power-line interference noise (50, 100 and 150 Hz) was eliminated by a notch filter (Hamming windowed FIR filter; EEGLAB: *pop_eegfiltnew* function). Epileptiform spikes in each hippocampal contact were automatically detected using the ISARG (Intracranial Signal Analysis Research Group) method with default settings[73] (http://isarg.fel.cvut.cz, version 16). We removed ripples that occurred within a time interval of 100 ms from each epileptiform spike to avoid detections of artifact ripples. We also presented the grand average of the epileptiform spike-locked raw signal and spectrogram for all detected IEDs during NREM sleep and wakefulness (Fig. S22).

EEG recordings for off-line sleep stage identification

To precisely identify each sleep stage, additional electrodes were placed on the scalp according to the 10-20 system and on the face for monitoring electrooculographic (EOG). In all, there were eight scalp electrodes (F3, F4, C3, C4, O1, O2, A1, A2), and two EOG electrodes (at the outer canthi of both eyes). If one of these electrodes could not be placed due to clinical reasons, we selected a nearby electrode to replace it (6 patients). To verify that the majority of cues were presented during NREM sleep, offline sleep staging was performed according to the criteria of the American Academy of Sleep Medicine (AASM) for non-overlapping time windows of 30 s, as shown in Table S3.

Index of memory change score

For each item, we calculated the memory change score according to three positions: the correct position for each item, the indicated position during the pre-sleep test and the indicated position during the post-sleep test.

$$Memory\ change\ score_{(i,j)} = \frac{a_{(i,j)} - b_{(i,j)}}{a_{(i,j)} + b_{(i,j)}} \quad (1)$$

$a_{(i,j)}$: Euclidean distance between the indicated position during the pre-sleep test and the correct position for jth participant's ith item (i = 1, 2, …50; j = 1, 2, …11). $b_{(i,j)}$: Euclidean distance between the indicated position during the post-sleep test and the correct position for jth participant's ith item. For 25 cued items of each subject, we classified the top 1/3 (rounded up to 9 items) as memory-strengthening items and the last 1/3 (rounded up to 9 items) as memory-decaying items according to their relative memory change score. The rest (7 items) are used as middle items (Fig. S1B).

Off-line ripple detection

Ripple detection was performed using electrode contacts located in the hippocampus (the exact anatomical location is depicted in Fig. 1F). For each participant, the hippocampal contact with the highest probability of being located in the hippocampus during the automatic brain segmentation procedure was used for ripple detection. We used previously published ripple detection scripts to detect ripple events[41] both during learning and sleep. Before the detection of ripple events, we implemented a process to reduce common noise by subtracting a reference signal obtained from a nearby white-matter contact. Subsequently, we filtered the local field potentials (LFPs) within the frequency range of 70 to 180 Hz using a Hamming windowed sinc FIR filter with a transition bandwidth of 5 Hz. We then calculated the analytic amplitude of the LFPs using a Hilbert transform. To minimize ripple-rate-induced biasing, the extreme values were robustly estimated using Least-Median-Squares and clipped to 4 SD above the mean value. After clipping the extreme values, the clipped signal was then squared and smoothed using a FIR low-pass filter with a 40 Hz cutoff frequency. Ripple events were identified from the original signal (squared but unclipped) when they exceeded 4 SD above the clipped signal. Event duration was expanded until ripple power fell below 2 SD. Events that were shorter than 20 milliseconds or longer than 200 milliseconds were excluded from further analysis. To avoid inclusion of possible pathological events, we removed any ripple events that occurred within 100 ms from inter-ictal epileptic discharges (IEDs).

Off-line spindle detection

Spindle events during TMR stage were detected for each gray-matter contact based on established detection algorithms[76,77]. To enhance data quality, we initially applied a noise reduction technique by subtracting a reference signal obtained from a nearby white-matter contact. Subsequently, the data underwent a bandpass filtering operation within the frequency range of 12 to 16 Hz (Hamming windowed sinc FIR filter). Next, we used Hilbert transform to obtain the instantaneous amplitude and computed a smoothed envelope with convolving by a Gaussian window (200 ms). The spindle amplitude criterion was then established as the 75th percentile of this smoothed envelope. Finally, spindle events were identified whenever the signal exceeded this threshold for a duration of more than 0.5 seconds but less than 3 s.

Ripple and spindle occurrence rate

To calculate the ripple and spindle occurrence rate, we assigned a value of 1 to the time points where the ripple/spindle was detected and 0 otherwise. Subsequently, we calculated the mean values across trials for each time point within the time range of [0–5 s] relative to the TMR cue onset as in Fig. S14 ([0–2 s] relative to the cue onset for learning ripple events as in Fig. S2). To eliminate the impact of individual variance on statistics, we normalized the ripple/spindle occurrence rate at each contact for each subject. We divided the occurrence rate after the cue onset by the average occurrence rate during the corresponding phase (e.g., awake ripple rate was divided by average ripple occurrence rate during learning stage).

Time-frequency analysis

Spectral decomposition of LFP data (learning stage and TMR stage) for all cortical and hippocampal contacts was done using Morlet wavelets (seven cycles, frequency bin: 2 Hz, step size: 20 ms) implemented in Fieldtrip. This spectrum was used to perform RSA. We used a finer time-frequency resolution (frequency bin: 0.5 Hz, step size: 10 ms) to obtain the cue-triggered power response during TMR stage. As a previous study had found the cue-evoked increase of pattern replay lasted for 10s[19], it was difficult to find a pure baseline before each cue in this study. Therefore, we normalized the spectrum using Z-score across all time bins at each frequency and contact (i.e., first performing log

transformation, then subtracting the mean value and dividing by the standard deviation across time).

The high-frequency broadband signal has been established as a reliable electrophysiological marker for local neuronal spiking activity, as indicated in previous studies[78–80]. Consistent with previous study[26], we calculated the mean normalized power within the HFB (60–160 Hz), averaged over a time window spanning from −250 ms to +250 ms relative to the occurrence of hippocampal ripple events. This approach was employed to capture ripple-coupled cortical activations in the current study.

Representational similarity analysis

As previous studies used slightly different frequency bands to generate distributed brain patterns (30–90 Hz[3] or 60–140 Hz[41]), we first determined the optimal frequency band by identifying item-specific activity patterns during learning stage (Fig. S20). Then we identified item-specific activity patterns, using a similar approach as in a previous iEEG study[3]. First, we applied an average reference including all iEEG contacts except for hippocampal contacts, in order to exclude an influence of hippocampal ripple activity. Second, we conducted a time-frequency transformation using Morlet wavelets to extract power values. Third, we normalized the iEEG power using Z-score across all time bins at each frequency and averaged the Z-score power within 50–140 Hz. Fourth, the normalized data were smoothed by a 4-point triangular window, resulting in a matrix of normalized 2D data [time × contacts] for learning stage and TMR stage which was used in the following analysis.

Retrieval-retrieval similarity (RRS) during learning stage. Previous studies indicated that ripples played an important role in the reactivation of mnemonic information[3,41,49]. In current study, we found that ripple rate increased when participants were asked to retrieve the object location (Fig. 2F). We further investigated whether item level representations can be observed around the occurrence of learning-related ripples (LR-ripple), defined as ripples occurred within 1.5 s window after image onset. We first extracted epochs of whole-brain data during a period from 500 ms before to 500 ms after LR-ripple onset, resulting in 2D data [time × contacts] for each trial (in cases where multiple ripples occurred in one trial, we selected the first ripple). Within-Item (WI) similarity was calculated as the whole-brain pattern similarity between trial pairs with the same item in different learning round, using Spearman's correlations. Between-Items (BI) similarity was calculated as the pattern similarity between trial pairs with different items in different learning round. The number of trials for each participant was reported in Table S6. All the similarity matrices were then Fisher Z-transformed. Subsequently, we averaged the WI similarity and BI similarity across trial pairs within each subject and compared them by conducting a paired-sample t-test across subjects.

Retrieval-sleep similarity (RSS) during TMR stage. We calculated the representational similarity between cortical activity around LR-ripple onset and cortical activity after TMR cues during sleep. As our RRS analysis confirmed that the whole brain pattern around the occurrence of hippocampal ripple contained item-specific information, we further examined whether this item-specific information was reactivated after TMR cues. Specifically, we first extracted epochs of whole-brain data ±500 ms around each LR-ripple onset, then correlated it with high-gamma activity (50–140 Hz) from TMR cue onset to 5000 ms afterwards (Fig. 3A). All the similarity matrices were fisher Z-transformed and smoothed by a 2D Gaussian smoothing kernel (σ = 40 ms) before further analysis. We then averaged data across all LR-ripple epochs of the same item, resulting in 3D RSS data [items × $time_{ripple}$ × $time_{cue}$].

Since the TMR was displayed for six rounds, we further checked the stability of the reactivation pattern for each round. The stability of the reactivation pattern was assessed by calculating the average Rho between the RSS matrix and behavioral performance across subjects

for each round (Fig. S6). To evaluate the consistency between each round and the main result, we correlated the RSS matrix of each round to the average RSS matrix of the rest five rounds. Rotations were performed on the matrices, and the similarity was computed to generate a distribution of shuffled data (Fig. S7). We also evaluated the stability of the reactivation pattern for individual subject using the similar procedure (Fig. S8 and S9, respectively).

We used two approaches to investigate the relation between RSS and behavioral performance: 1) we incorporated all items to compute the Spearman correlation (Rho) between the RSS matrix and behavioral performance for each subject. To assess the significance, a cluster-based permutation test was performed by shuffling the memory change score within each subject and repeating the above procedure 1000 times (Fig. 3). 2) According to each item's memory change score, we extracted RSS for strengthening and decaying items separately (i.e., $RSS_{strengthening}$ and $RSS_{decaying}$). Subsequently, we averaged the $RSS_{strengthening}$ and $RSS_{decaying}$ across items within each subject and compared them by conducting a paired-sample t-test across subjects. We shuffled the conditional labels 1000 times to obtain significant clusters between $RSS_{strengthening}$ and $RSS_{decaying}$ (Fig. 4B).

Connectivity analysis

We quantified the synchronization of brain activity patterns during TMR and assessed the difference between strengthening and decaying item representations by calculating spectral coherence between all hippocampal contacts and cortical contacts. For each participant, the data matrix (contacts × time × TMR cues) was extracted between the onset of TMR cues to 5000 ms afterwards. Then this data matrix was divided into a $data_{strengthening}$ (contacts × time × $epochs_{strengthening}$) and a $data_{decaying}$ (contacts × time × $epochs_{decaying}$) depending on memory change scores. Similarly, we used the trials of guitar strum as $data_{control}$ (contacts × time × $epochs_{guitar\ strum}$). For each participant and each condition (strengthening, decaying and control), the number of trials between the conditions was balanced (Table S6). The coherence between time-series of x(t) and y(t) was then estimated as a function of frequency:

$$C(x,y,t,f) = \frac{|S(x,y,t,f)|^2}{S(x,x,t,f)S(y,y,t,f)} \quad (2)$$

where $S(x,x,t,f)$ and $S(y,y,t,f)$ are the power spectral densities of x-th hippocampal contact and y-th cortical contact in the t-th time window (window size: 1000 ms, step size: 62.5 ms), respectively, and $S(x,y,t,f)$ is the cross-spectral density between two contacts in t-th time window. We averaged the coherence across hippocampal contacts to yield hippocampal-cortical coherence ($contacts_{cortex}$ × time × frequency).

To investigate the difference in coherence between the strengthening, decaying and control condition, we selected two temporal windows according to 1st reactivation and 2nd reactivation found in the analysis of RSA (Fig. 4B, 1st reactivation: 1.6–2.6 s and 2nd reactivation: 2.8–3.8 s). Then hippocampal-cortical coherence was averaged across time range and cluster-based permutation test was performed to find significant frequency bands (Fig. 5A, E).

Statistical analysis

To handle the case where the predictor variables were not independent[81], we used the linear mixed effect model (LME) (*fitlme* function in MATLAB) and the restricted maximum likelihood method for statistical analysis. To assess the effects of condition (e.g., strengthening versus decaying) on coherence and cortical HFB power, we implemented an LME model with subjects and contact pairs as two

(nested) random effects:

$$Y \sim condition + (1 \mid subjects) + (1 \mid subjects : contacts) \qquad (3)$$

where the dependent variable Y is either coherence or HFB power. The condition variable is coded as 0 for decaying and 1 for strengthening.

For cluster-based permutation tests, we first performed paired t-tests, LME model or nonparametric test and then identified clusters based on a threshold (i.e., for ripple rate and RSA: $p < 0.05$; others: $p < 0.01$) and summed the t-values within the clusters. We then shuffled condition labels, repeated the above operation 1000 times, and extracted the largest cluster in each permutation. Finally, we determined the significance of an original cluster's t-value according to its order among the 1000 permutations.

Reporting summary
Further information on research design is available in the Nature Portfolio Reporting Summary linked to this article.

Data availability
The processed data in this study are available via: https://doi.org/10.5281/zenodo.14583770. The raw data are available via: https://doi.org/10.5281/zenodo.14885381. Source data are provided with this paper.

Code availability
We used the Matlab code from https://doi.org/10.5281/zenodo.3259369, based on Yitzhak Norman and associates' work to detect ripple. Code of representational similarity analysis and statistical test are available via: https://doi.org/10.5281/zenodo.14583770. The code to reproduce all figures is also included in the link above.

References
1. Rothschild, G., Eban, E. & Frank, L. M. A cortical-hippocampal-cortical loop of information processing during memory consolidation. *Nat. Neurosci.* **20**, 251–259 (2017).
2. Staresina, B. P., Niediek, J., Borger, V., Surges, R., & Mormann, F. How coupled slow oscillations, spindles and ripples coordinate neuronal processing and communication during human sleep. *Nat. Neurosci.* https://doi.org/10.1038/s41593-023-01381-w (2023).
3. Zhang, H., Fell, J. & Axmacher, N. Electrophysiological mechanisms of human memory consolidation. *Nat. Commun.* **9**, 4103 (2018).
4. Geva-Sagiv, M. et al. Augmenting hippocampal-prefrontal neuronal synchrony during sleep enhances memory consolidation in humans. *Nat. Neurosci.* **26**, 1100–1110 (2023).
5. Stickgold, R. & Walker, M. P. Sleep-dependent memory triage: evolving generalization through selective processing. *Nat. Neurosci.* **16**, 139–145 (2013).
6. Wilhelm, I. et al. Sleep selectively enhances memory expected to be of future relevance. *J. Neurosci.* **31**, 1563–1569 (2011).
7. Sterpenich, V. et al. Reward biases spontaneous neural reactivation during sleep. *Nat. Commun.* **12**, 4162 (2021).
8. Sterpenich, V. et al. Sleep promotes the neural reorganization of remote emotional memory. *J. Neurosci.* **29**, 5143–5152 (2009).
9. Nishida, M., Pearsall, J., Buckner, R. L. & Walker, M. P. REM sleep, prefrontal theta, and the consolidation of human emotional memory. *Cereb. Cortex* **19**, 1158–1166 (2009).
10. Fischer, S. & Born, J. Anticipated reward enhances offline learning during sleep. *J. Exp. Psychol. Learn Mem. Cogn.* **35**, 1586–1593 (2009).
11. Hu, X., Cheng, L. Y., Chiu, M. H. & Paller, K. A. Promoting memory consolidation during sleep: A meta-analysis of targeted memory reactivation. *Psychol. Bull.* **146**, 218–244 (2020).
12. Lewis, P. A. & Bendor, D. How targeted memory reactivation promotes the selective strengthening of memories in Sleep. *Curr. Biol.* **29**, R906–R912 (2019).
13. Rudoy, J. D., Voss, J. L., Westerberg, C. E. & Paller, K. A. Strengthening individual memories by reactivating them during sleep. *Science* **326**, 1079 (2009).
14. Rasch, B., Buchel, C., Gais, S. & Born, J. Odor cues during slow-wave sleep prompt declarative memory consolidation. *Science* **315**, 1426–1429 (2007).
15. Schreiner, T., Petzka, M., Staudigl, T. & Staresina, B. P. Endogenous memory reactivation during sleep in humans is clocked by slow oscillation-spindle complexes. *Nat. Commun.* **12**. https://doi.org/10.1038/s41467-021-23520-2 (2021).
16. Shanahan, L. K., Gjorgieva, E., Paller, K. A., Kahnt, T. & Gottfried, J. A. Odor-evoked category reactivation in human ventromedial prefrontal cortex during sleep promotes memory consolidation. *Elife* **7**. https://doi.org/10.7554/eLife.39681 (2018).
17. Cairney, S. A., Guttesen, A. A. V., El Marj, N. & Staresina, B. P. Memory consolidation is linked to spindle-mediated information processing during sleep. *Curr. Biol.* **28**, 948–954 e944 (2018).
18. Belal, S. et al. Identification of memory reactivation during sleep by EEG classification. *Neuroimage* **176**, 203–214 (2018).
19. Bendor, D. & Wilson, M. A. Biasing the content of hippocampal replay during sleep. *Nat. Neurosci.* **15**, 1439–1444 (2012).
20. Schreiner, T., Doeller, C. F., Jensen, O., Rasch, B. & Staudigl, T. Theta phase-coordinated memory reactivation reoccurs in a slow-oscillatory rhythm during NREM sleep. *Cell Rep.* **25**, 296–301 (2018).
21. Buzsaki, G. Hippocampal sharp wave-ripple: a cognitive biomarker for episodic memory and planning. *Hippocampus* **25**, 1073–1188 (2015).
22. Klinzing, J. G., Niethard, N. & Born, J. Mechanisms of systems memory consolidation during sleep. *Nat. Neurosci.* **22**, 1598–1610 (2019).
23. Mednick, S. C. et al. The critical role of sleep spindles in hippocampal-dependent memory: a pharmacology study. *J. Neurosci.* **33**, 4494–4504 (2013).
24. Khodagholy, D., Gelinas, J. N. & Buzsáki, G. Learning-enhanced coupling between ripple oscillations in association cortices and hippocampus. *Science* **358**, 369–372 (2017).
25. Lewis, P. A. & Durrant, S. J. Overlapping memory replay during sleep builds cognitive schemata. *Trends Cogn. Sci.* **15**, 343–351 (2011).
26. Norman, Y., Raccah, O., Liu, S., Parvizi, J. & Malach, R. Hippocampal ripples and their coordinated dialogue with the default mode network during recent and remote recollection. *Neuron* **109**, 2767–2780 e2765 (2021).
27. Vaz, A. P., Inati, S. K., Brunel, N. & Zaghloul, K. A. Coupled ripple oscillations between the medial temporal lobe and neocortex retrieve human memory. *Science* **363**, 975–978 (2019).
28. Liu, J. et al. Stable maintenance of multiple representational formats in human visual short-term memory. *Proc. Natl Acad. Sci. USA* **117**, 32329–32339 (2020).
29. Yaffe, R. B. et al. Reinstatement of distributed cortical oscillations occurs with precise spatiotemporal dynamics during successful memory retrieval. *Proc. Natl Acad. Sci. USA* **111**, 18727–18732 (2014).
30. Tonegawa, S., Morrissey, M. D. & Kitamura, T. The role of engram cells in the systems consolidation of memory. *Nat. Rev. Neurosci.* **19**, 485–498 (2018).
31. Rasch, B. & Born, J. About sleep's role in memory. *Physiol. Rev.* **93**, 681–766 (2013).
32. Brodt, S., Inostroza, M., Niethard, N. & Born, J. Sleep-A brain-state serving systems memory consolidation. *Neuron* **111**, 1050–1075 (2023).
33. Berkers, R. et al. Cued reactivation during slow-wave sleep induces brain connectivity changes related to memory stabilization. *Sci. Rep.* **8**, 16958 (2018).

34. van Dongen, E. V. et al. Memory stabilization with targeted reactivation during human slow-wave sleep. *Proc. Natl Acad. Sci. USA* **109**, 10575–10580 (2012).

35. Cousins, J. N., El-Deredy, W., Parkes, L. M., Hennies, N. & Lewis, P. A. Cued reactivation of motor learning during sleep leads to overnight changes in functional brain activity and connectivity. *PLoS Biol.* **14**, e1002451 (2016).

36. Creery, J. D., Oudiette, D., Antony, J. W. & Paller, K. A. Targeted memory reactivation during sleep depends on prior learning. *Sleep* **38**, 755–763 (2015).

37. Creery, J. D. et al. Electrophysiological markers of memory consolidation in the human brain when memories are reactivated during sleep. 119, e2123430119.

38. Wang, B. et al. Targeted memory reactivation during sleep elicits neural signals related to learning content. *J. Neurosci.* **39**, 6728–6736 (2019).

39. Antony, J. W., Cheng, L. Y., Brooks, P. P., Paller, K. A. & Norman, K. A. Competitive learning modulates memory consolidation during sleep. *Neurobiol. Learn. Mem.* **155**, 216–230 (2018).

40. Antony, J. W. et al. Sleep spindle refractoriness segregates periods of memory reactivation. *Curr. Biol.* **28**, 1736–1743.e1734 (2017).

41. Norman, Y. et al. Hippocampal sharp-wave ripples linked to visual episodic recollection in humans. *Science*, 365. https://doi.org/10.1126/science.aax1030 (2019).

42. Buzsáki, G., Horváth, Z., Urioste, R., Hetke, J. & Wise, K. High-frequency network oscillation in the hippocampus. *Science* **256**, 1025–1027 (1992).

43. Buzsáki, G. et al. Hippocampal network patterns of activity in the mouse. *Neuroscience* **116**, 201–211 (2003).

44. Ylinen, A. et al. Sharp wave-associated high-frequency oscillation (200 hz) in the intact hippocampus: Network and intracellular mechanisms. *J. Neurosci.* **15**, 30–46 (1995).

45. Liu, A. A. et al. A consensus statement on detection of hippocampal sharp wave ripples and differentiation from other fast oscillations. *Nature Communications* **13**. https://doi.org/10.1038/s41467-022-33536-x (2022).

46. van Schalkwijk, F. J. et al. An evolutionary conserved division-of-labor between archicortical and neocortical ripples organizes information transfer during sleep. *Prog. Neurobiol.* **227**, 102485 (2023).

47. Buzsaki, G. & Draguhn, A. Neuronal oscillations in cortical networks. *Science* **304**, 1926–1929 (2004).

48. Buzsáki, G., Logothetis, N. & Singer, W. Scaling brain size, keeping timing: evolutionary preservation of brain rhythms. *Neuron* **80**, 751–764 (2013).

49. Liu, Y., Dolan, R. J., Kurth-Nelson, Z. & Behrens, T. E. J. Human replay spontaneously reorganizes experience. *Cell* **178**, 640–652 e614 (2019).

50. Liu, J. et al. Item-specific neural representations during human sleep support long-term memory. *PLoS Biol.* **21**, e3002399 (2023).

51. Wen, H. & Liu, Z. Separating fractal and oscillatory components in the power spectrum of neurophysiological signal. *Brain Topogr.* **29**, 13–26 (2016).

52. Schreiner, T. et al. Spindle-locked ripples mediate memory reactivation during human NREM sleep. *Nat. Commun.* **15**, 5249 (2024).

53. Joo, H. R. & Frank, L. M. The hippocampal sharp wave-ripple in memory retrieval for immediate use and consolidation. *Nat. Rev. Neurosci.* **19**, 744–757 (2018).

54. Roumis, D. K. & Frank, L. M. Hippocampal sharp-wave ripples in waking and sleeping states. *Curr. Opin. Neurobiol.* **35**, 6–12 (2015).

55. Girardeau, G., Benchenane, K., Wiener, S. I., Buzsáki, G. & Zugaro, M. B. Selective suppression of hippocampal ripples impairs spatial memory. *Nat. Neurosci.* **12**, 1222–1223 (2009).

56. Dickey, C. W. et al. Widespread ripples synchronize human cortical activity during sleep, waking, and memory recall. *Proc. Natl Acad. Sci. USA* **119**, e2107797119 (2022).

57. Clemens, Z. et al. Temporal coupling of parahippocampal ripples, sleep spindles and slow oscillations in humans. *Brain* **130**, 2868–2878 (2007).

58. Staba, R. J. et al. High-frequency oscillations recorded in human medial temporal lobe during sleep. *Ann. Neurol.* **56**, 108–115 (2004).

59. Axmacher, N., Elger, C. E. & Fell, J. Ripples in the medial temporal lobe are relevant for human memory consolidation. *Brain* **131**, 1806–1817 (2008).

60. Jadhav, S. P., Rothschild, G., Roumis, D. K. & Frank, L. M. Coordinated excitation and inhibition of prefrontal ensembles during awake hippocampal sharp-wave ripple events. *Neuron* **90**, 113–127 (2016).

61. Ji, D. & Wilson, M. A. Coordinated memory replay in the visual cortex and hippocampus during sleep. *Nat. Neurosci.* **10**, 100–107 (2007).

62. Peyrache, A., Khamassi, M., Benchenane, K., Wiener, S. I. & Battaglia, F. P. Replay of rule-learning related neural patterns in the prefrontal cortex during sleep. *Nat. Neurosci.* **12**, 919–926 (2009).

63. Wierzynski, C. M., Lubenov, E. V., Gu, M. & Siapas, A. G. State-dependent spike-timing relationships between hippocampal and prefrontal circuits during sleep. *Neuron* **61**, 587–596 (2009).

64. Squire, L. R. Memory and the hippocampus: a synthesis from findings with rats, monkeys, and humans. *Psychol. Rev.* **99**, 195–231 (1992).

65. Squire, L. R., Cohen, N. J., & Nadel, L. The medial temporal region and memory consolidation: A new hypothesis. In *Memory Consolidation: Psychobiology of Cognition*, 185–210 (1984).

66. Ameen, M., Jacobs, J., Schabus, M., Hoedlmoser, K., & Donoghue, T. *The Temporal Dynamics of Aperiodic Neural Activity Track Changes in Sleep Architecture.* https://doi.org/10.1101/2024.01.25.577204 (2024)

67. Bódizs, R. et al. Fundamentals of sleep regulation: model and benchmark values for fractal and oscillatory neurodynamics. *Prog. Neurobiol.* **234**. https://doi.org/10.1016/j.pneurobio.2024.102589 (2024).

68. Donoghue, T. et al. Parameterizing neural power spectra into periodic and aperiodic components. *Nat. Neurosci.* **23**, 1655–1665 (2020).

69. Lendner, J. D. et al. An electrophysiological marker of arousal level in humans. *Elife* **9**. https://doi.org/10.7554/eLife.55092 (2020).

70. Oudiette, D. & Paller, K. A. Upgrading the sleeping brain with targeted memory reactivation. *Trends Cogn. Sci.* **17**, 142–149 (2013).

71. Delorme, A. & Makeig, S. EEGLAB: an open source toolbox for analysis of single-trial EEG dynamics including independent component analysis. *J. Neurosci. Methods* **134**, 9–21 (2004).

72. Oostenveld, R., Fries, P., Maris, E. & Schoffelen, J. M. FieldTrip: Open source software for advanced analysis of MEG, EEG, and invasive electrophysiological data. *Comput Intell. Neurosci.* **2011**, 156869 (2011).

73. Janca, R. et al. Detection of interictal epileptiform discharges using signal envelope distribution modelling: application to epileptic and non-epileptic intracranial recordings. *Brain Topogr.* **28**, 172–183 (2015).

74. Qin, C. et al. Automatic and Precise Localization and Cortical Labeling of Subdural and Depth Intracranial Electrodes. *Front Neuroinform* **11**, 10 (2017).

75. Desikan, R. S. et al. An automated labeling system for subdividing the human cerebral cortex on MRI scans into gyral based regions of interest. *Neuroimage* **31**, 968–980 (2006).

76. Staresina, B. P. et al. Hierarchical nesting of slow oscillations, spindles and ripples in the human hippocampus during sleep. *Nat. Neurosci.* **18**, 1679–1686 (2015).

77. Kim, J., Gulati, T. & Ganguly, K. Competing roles of slow oscillations and delta waves in memory consolidation versus forgetting. *Cell* **179**, 514–526 e513 (2019).

78. Mukamel, R. et al. Coupling between neuronal firing, field potentials, and FMRI in human auditory cortex. *Science* **309**, 951–954 (2005).

79. Parvizi, J. & Kastner, S. Promises and limitations of human intracranial electroencephalography. *Nat. Neurosci.* **21**, 474–483 (2018).

80. Watson, B. O., Ding, M. & Buzsáki, G. Temporal coupling of field potentials and action potentials in the neocortex. *Eur. J. Neurosci.* **48**, 2482–2497 (2018).

81. Patterson, H. D. & Thompson, R. Recovery of Inter-Block Information When Block Sizes are Unequal. *Biometrika* **58**, 545–554 (1971).

Acknowledgements

Author contributions

Conceptualization: L.W., Z.X.; Data acquisition: W.D., Z.X.; Data resources: J.W., M.W.; Data Analysis: W.D., X.X., D.C., P.L., Z.T.; Writing–original draft: Z.X., W.D.; Writing review & editing: L.W., W.D., Z.X., D.C., J.L., N.A., K.A.P.; Funding acquisition: L.W., N.A.

Competing interests

The authors declare no competing interests.

Additional information

Supplementary information The online version contains supplementary material available at https://doi.org/10.1038/s41467-025-57766-x.

Correspondence and requests for materials should be addressed to Liang Wang.

Peer review information *Nature Communications* thanks the anonymous reviewer(s) for their contribution to the peer review of this work. A peer review file is available.

Reprints and permissions information is available at http://www.nature.com/reprints

Publisher's note Springer Nature remains neutral with regard to jurisdictional claims in published maps and institutional affiliations.